Int. J. Electrochem. Sci., 8 **(2013)** 135 - 148

International Journal of
ELECTROCHEMICAL
SCIENCE
www.electrochemsci.org

One-step Construction of Sensor Based on Nanocomposite of Platinum and Chitosan Formed by Electrodeposition and Its Application for Determination of Nitrite

Xiaohong Zhu[*], *Aimin Ding*

Department of Chemistry and Chemical Engineering , Hefei Normal University Hefei 230061, P. R. China
[*]E-mail: zhuxh@mail.ustc.edu.cn

Received: 31 October 2012 / *Accepted:* 4 December 2012 / *Published:* 1 January 2013

A novel platinum–chitosan nano-composite (Pt-CS) was synthesized by electrochemical co-deposition at a glassy carbon electrode (GCE) for fabrication of a nitrite sensor, Pt-CS/GCE. The deposition formed a nanocomposite modified surface layer on the GCE, which was characterized by X-ray photoelectron spectroscopy (XPS), X-ray diffraction (XRD) and field emission scanning electron microscope (SEM). It was found that the Pt-CS nano-composite generated flower-like spherical particles with sizes of about 250 nm, which was consisted of Pt nanoparticles with sizes smaller than 10 nm, suggesting that the chitosan molecules were covered on the surface of Pt nanoparticles to form a core-shell structure. The electrocatalytic activity and sensing ability of the modified electrode was investigated by cyclic voltammetry (CV), differential pulse voltammetry (DPV) and differential pulse amperometry (DPA). It demonstrated that the electrode was excellent for catalytic determination of nitrite with good reproducibility, good stability and fast response. The detection limit was found to be 1.5×10^{-7} M and the linear concentration range is 9.9×10^{-7} to 7.5×10^{-3} M.

Keywords: nanocomposite, nitrite, electrodeposition, modified electrodes,

1. INTRODUCTION

Noble metal nanoparticles have been extensively utilized owing to their extraordinary catalytic activities. Particularly, platinum nanoparticle-attached surfaces have been attracting extensive attention for fabrication of electrodes [1-3]. Several methods including chemical reduction [4], sputter deposition[5] and electrochemical deposition [6-8] have been developed for the preparation of platinum nanoparticles. The platinum nanoparticles produced by reduction of platinum tetrachloride with $NaBH_4$ in the presence of chitosan can generate the platinum–chitosan (Pt-CS) nanocomposites [9], in which the chitosan molecules were adsorbed onto the surface of the platinum nanoparticles

since chitosan is a strong chelating agent for metals. The stabilization of metal nanoparticles with chitosan has been extensively reported [10, 11]. This property was making it particularly useful in sensor development [12, 13].

One-step generation of nanocomposite has recently been demonstrated as simple and efficient method for fabrication various electrochemical sensors [14-16]. However, to the best of our knowledge, there has been no report focused on the simple one-step electrochemically generated interface containing Pt-CS nanocomposites for sensing purpose. In this work, we investigated the in-situ fabrication of Pt-CS nano-composites with controllable dimensions on the electrode surface directly by cyclic voltammetry. The obtained electrode exhibited high stability and remarkable catalytic activity for the oxidation of nitrite.

2. EXPERIMENTAL SECTION

Chemicals. H_2PtCl_4, KCl, $NaNO_2$, K_2HPO_4, KH_2PO_4, $NaNO_3$,$CaCl_2$, $Mg(NO_3)_2$, ascorbic acid and uric acid were of analytical grade and purchased from Shanghai chemical Reagents (China). Dopamine was purchased from Sigma (USA) and used as received without further purification. Doubly distilled water and high purity nitrogen were used. Phosphate buffered solutions (PBS, 0.1 M) containing 0.1 M KCl were prepared as the supporting electrolyte.

Instruments. A JSM-6700F (JEOL) Field Emission Scanning Electron microanalyser (FE-SEM) was used to examine the morphologies. Surface analysis of the electrodes was performed by X-ray photoelectron spectroscopy (XPS) on ESCALAB MKII spectrometer (VG Co., UK) with a Mg Kα radiation as the exciting source. X-ray diffraction (XRD) was recorded on a philips X'pert Pro X-ray diffractometer (Philips Company, Holand) using a Cu Kα radiation (λ= 0. 154 056 nm).

Cyclic voltammetry (CV), differential pulse voltammetry (DPV) and Differential pulse amperometry (DPA) were performed with a model CHI 832 electrochemical analyzer (Cheng-Hua Instruments Co, Shanghai, China). A conventional three-electrode system was used, which is consisted of a testing electrode, a platinum counter electrode, and a saturated calomel electrode (SCE) as the reference. Glassy carbon disk electrodes (GCE, Φ = 4.0 mm, formal surface area = 0.126 cm^2) (Lan-Like HCET Company, Tianjin, China) were used as the basal electrodes for the fabrication. Experiments were performed at room temperature (25^oC). The electrochemical solutions were thoroughly deoxygenated by N_2 bubbling before sampling and an N_2 atmosphere was maintained throughout the experiment. For DPA measurements, the solution was stirred by a magnetic stirrer. All potentials reported in this paper are versus SCE.

Electrode preparation. Prior to modification, the bare GCE was polished successively with 1.0, 0.3, 0.05 μm alumina slurries to a mirror finish. The electrode was rinsed with doubly distilled water after each polishing, and ultrasonicated in ethanol and water for 5 min, respectively. Then, the bare GCE was subjected to electrochemical deposition.

The deposition was accomplished with CV potential cycling in a solution. The experimental conditions were optimized as: potential cycling range: –0.5 V to 0.4 V; scan rate: 100 mV/s; cycle number: 40; deposition solution: freshly prepared solution of 2.0 mM H_2PtCl_4 + 0.5%(w/v) Chitosan

+1% acetic acid. Then, the electrode was further treated in 0.1 M pH 7.0 PBS + 0.1 M KCl by CV potential cycling between 0.2 and 1.2V for more than 10 cycles, until the CV profile becomes stable. The obtained electrode is denoted as Pt-CS/GCE. The electrode was stored in 0.1 M PBS before use.

Similarly, the above procedure was also performed for preparison of single platinum nanoclusters deposited electrode, denoted as Pt/GCE, by using the same experimental conditions except that the solutions contain no Chitosan.

3. RESULTS AND DISCUSSION

Generation of platinum–chitosan nanocomposites

Figure 1 shows the typical CV curves during the electrochemical deposition of Pt-CS nanocomposite on GCE. It can be seen from this figure that a pair of redox peaks(a_1, c_1)were growing up from cycle to cycle at a meddle potential (E_m) of −0.21V, which is indicative of the deposition and accumulation of Pt on the electrode surface.

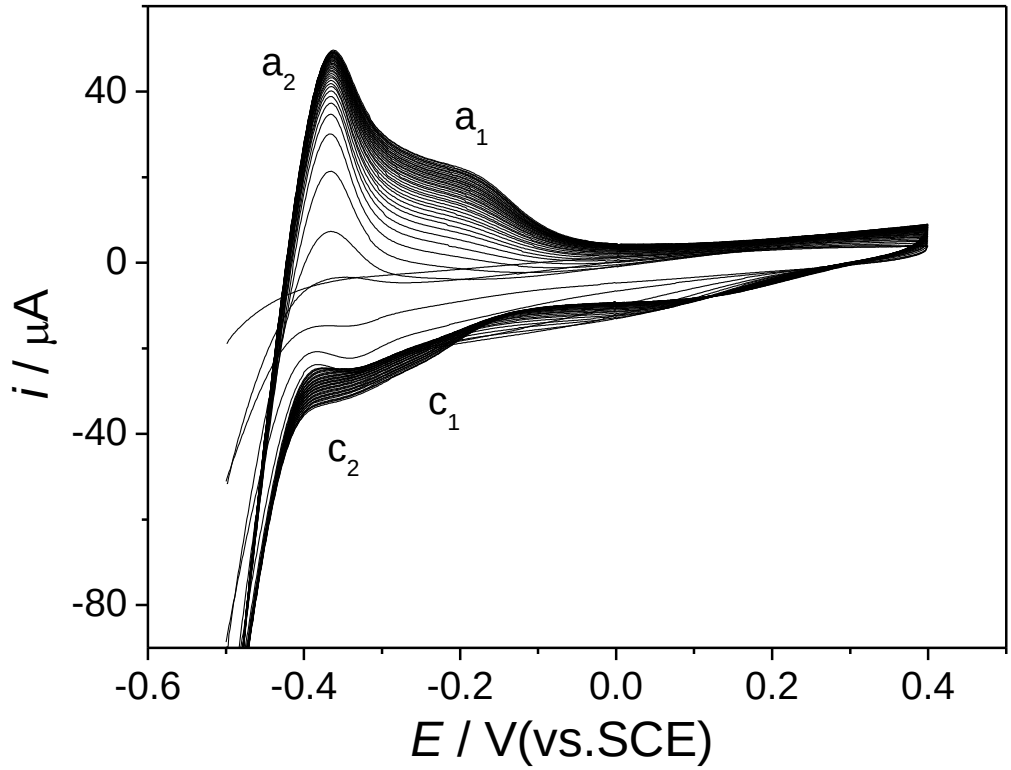

Figure 1. Multicycle CV of the electrodeposition process in 2.0 mM H_2PtCl_4 solution containing 0.5% chitosan at a scan rate of 100 mV/s.

The reaction mechanism of this redox couple can be attributed to the $PtCl_6^{2-}/PtCl_4^{2-}$ reduction and re-reduction processes followed by the $PtCl_4^{2-}$/Pt(0) redox step [17]. The shallow peak C_2 around -0.34V has been related to the reduction of hydrogen ions to hydrogen adatoms. At more cathodic

potentials the surface is saturated and hydrogen recombination with bulk hydrogen evolution occurs on already formed Pt nanoparticles. Peak a_2 on the returning branch of the CV is probably associated with the oxidation of some H_2 that has not yet diffused away from the Pt electrode after being formed.

Characterization of Pt-CS/GCE

Figure 2 shows the surface images of these prepared electrodes.

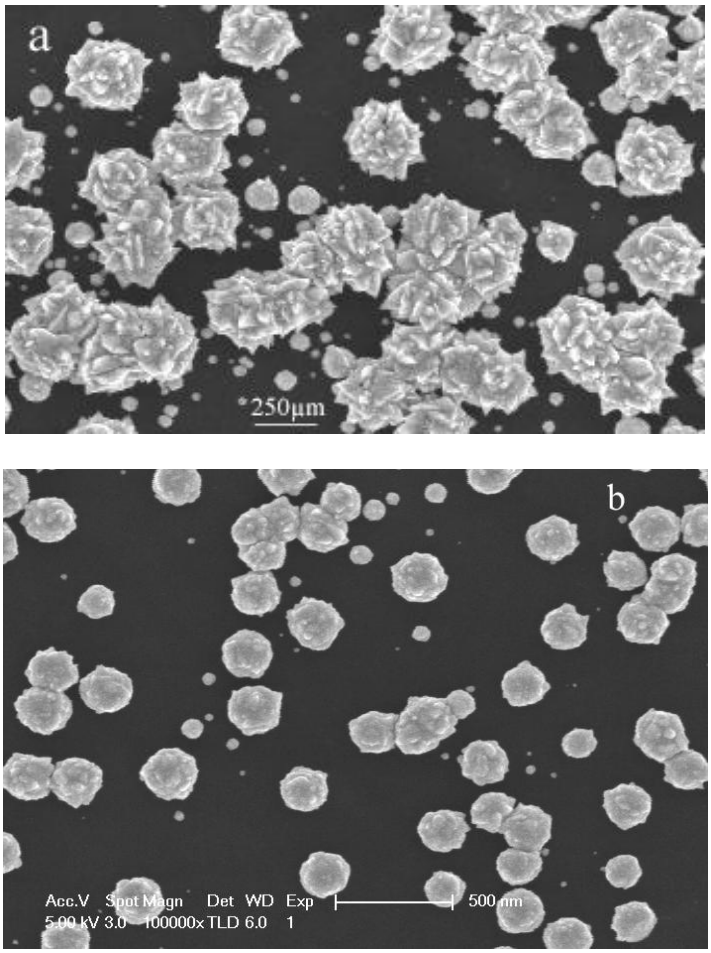

Figure 2. SEM images of the electrode surfaces: (a) Pt/GCE; (b) Pt-CS/GCE.

As can be seen from Fig. 2a, flower-like Pt nanoclusters were generated on the GCE substrate, which manifested that H_2PtCl_4 can be electrochemically reduced to Pt nanoparticles and deposited on the electrode surface at the applied conditions. The average size of the formed Pt nanoclusters is about 350 nm, which must be aggregate of much finer nanoparticles. It can be seen from Fig. 2b that the produced nanoclusters are also well distributed on the Pt-CS/GCE, while the size of the Pt-CS nanoclusters is about 250 nm, which is little smaller than that of Pt nanoclusters on the Pt/GCE shown in Fig. 2a. We have demonstrated that the CV deposition of Pt nanoparticles, in which a Pt nanoparticle was formed during one cycle of CV scan [18]. Similar cases can be expected to occur in the generation of Pt-CS nanoparticles. The Pt deposition occurs for the cathodic scanning beyond the potential of -0.21V, in which new Pt nanoparticles were generated, and the particles would be covered

by chitosan molecules by surface adsorption during the cathodic scan beyond the potential of -0.21V, generating a Pt-CS core-shell structure. The chitosan adsorption can be attributed to the free amino groups in chitosan, which contribute polycationic and chelating, along with ready solubility in weak acid [19, 20]. Chitosan adsorption on the surfaces of metal nanoparticles can stabilize and protect the nanoparticles [10]. In the present case, the coverage of chitosan on the newly generated Pt nanoparticles will prevent it from growing further in the next potential scans, and also stabilize the size and surface property of the Pt nanoparticles in the cluster during its applications. In other words, the CV deposition gives the advantage of entrapping the chitosan into the electrodeposited clusters of Pt to form a novel platinum–chitosan nanocomposite.

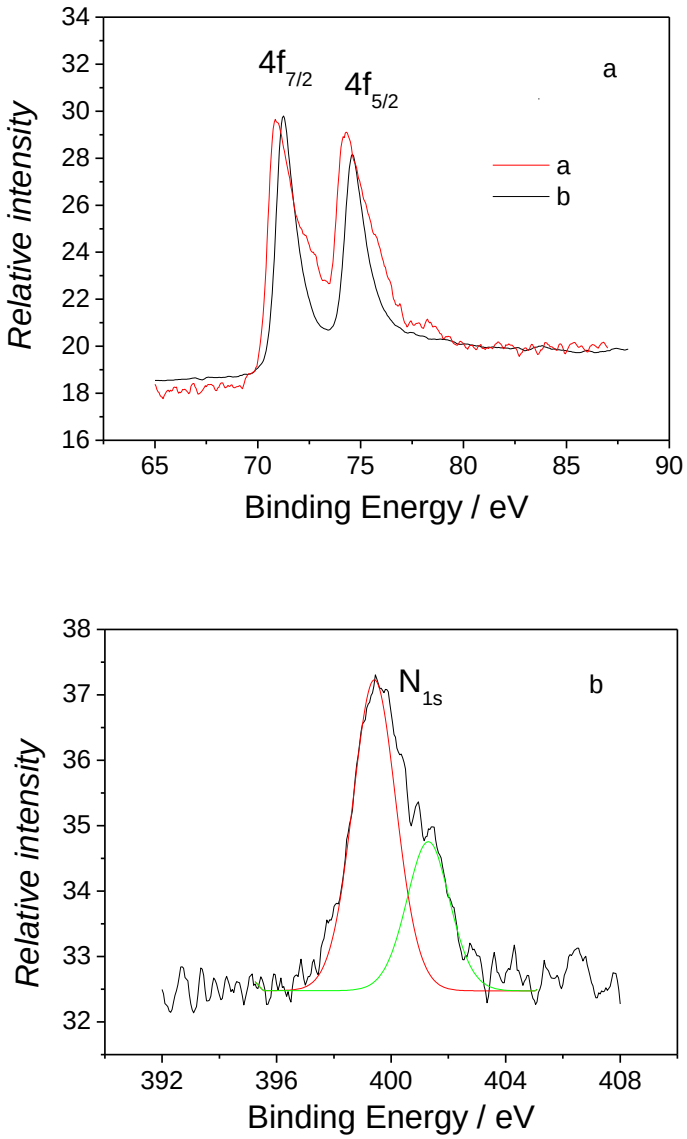

Figure 3. X-ray photoelectron spectra: (a) the 4f peaks for nano-Pt (curve a) and Pt-CS nano-composite (curve b); (b) the N 1s peak for Pt-CS/GCE.

The comparison of images in Figure 2 (a) and (b) shows that no more flower-like structure can be seen in the Pt-CS clusters, which is attributed to the chitosan coverage that may interfere the crystalline structure of the underlying particles.

To further verify the composite formation, the surface of Pt /GCE and Pt-CS /GCE was characterized by XPS, as shown in Figure 3. Figure 3(a) shows two peaks at binding energies (BE) 71.3 and 74.6 eV, these are the characteristic $4f_{7/2}$ and $4f_{5/2}$ peaks for Pt^0, and indicate the existence of Pt^0 in the surface layer. In comparison of curve b with curve a, we can see that the two peaks all shift to higher binding energies upon the Pt-CS composite formation, which is expected that the core level peaks of metal atoms can be shifted to higher binding energy by surrounding metal and partially nonmetal atoms [21]. Therefore, the observed peak shifts indicate the presence of the interaction between nano-Pt and chitosan.

Figure 3(b) shows the N1s peak at about 400 eV, which demonstrates that chitosan molecules on the surface. The peak can be deconvoluted into two peak components at 399.4 and 401.3 eV, attributed to —NH_2 and—NH_3^+ groups, respectively. The peak height ratio of these groups is about 1:2, indicating that one third of the amine groups was in the protonated state.

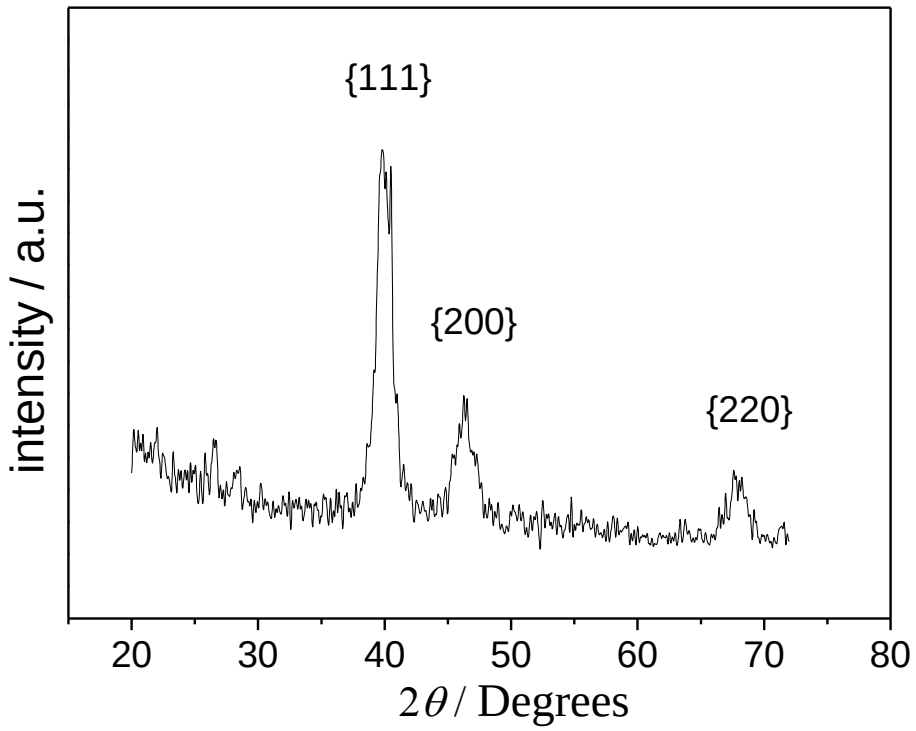

Figure 4. XRD patterns of Pt-CS/GCE.

The XRD pattern of the surface modified layer was obtained as shown in Fig.4. The diffraction pattern shows clearly three major peaks at 39.7°, 46.2° and 67.4°, which can be assigned to the diffraction from the {1 1 1}, {2 0 0} and {2 2 0} planes of the face-centered cubic lattice of Pt(0), respectively. Furthermore, the particle size of the Pt can be calculated according to Scherrer's equation

[22], $\beta = \kappa\lambda/D\cos\theta$, where λ is the X-ray wavelength, κ is the shape factor (0.89), β is the average diameter of the particles, θ is the Bragg angle in degree, and D is the full-width half-maximum of respective diffraction peak. Based on the D value of the reflection peak at 2θ of 39.7º, an averaged diameter of the Pt-CS nanoparticles was calculated as 8.5 nm.

Electrocatalytic oxidation of nitrite at Pt-CS /GCE

Cyclic voltammetry. The CV curves of nitrite at Pt-CS/GCE were presented in comparison with those obtained at Pt/GCE and a bare GCE as shown in Figure 5.

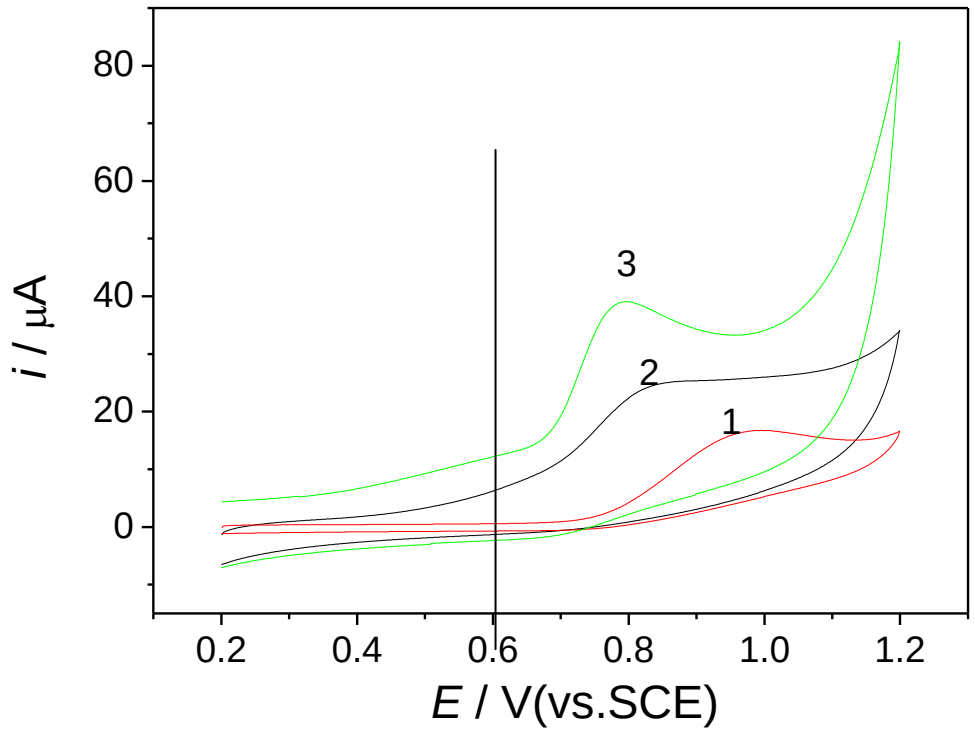

Figure 5. CV curves of (1) bare GCE, (2) Pt/GCE, (3) Pt-CS/GCE in 0.50 mM $NaNO_2$ + 0.1 M PBS (pH 6.0) at a scan rate of 50 mV/s.

It can be seen that the nitrite showed a broad small peak at the peak potential (E_p) of about 1.0 V at bare GCE. The Pt-CS/GCE and Pt/GCE gave oxidation peaks at about 0.80 and 0.85V, respectively, which is about 200 and 150 mV less positive than the peak at GCE. The anodic peak current at Pt-CS/GCE and at Pt/GCE can be estimated as 2.9-fold and 1.8-fold of the peak at GCE, respectively. The negative shifts of the peak potentials indicate the reductions of overpotentials of the nitrite oxidation reactions at the electrode surfaces, The electrocatalytic activity toward nitrite oxidation is in the order of Pt-CS/GCE > Pt/GCE > GCE. The current increase could be partially the result of the increase in reversibility of the electron transfer processes, which is evidenced from the decreases of the potential distance between E_p and the half peak potential ($E_{p/2}$). Moreover, we noted that these peaks showed different shapes, which may reflect different mass-transport mechanism at these electrodes. The current at GCE gave a regular curve for a planar diffusion controlled process. The curve at Pt/GCE gave a current plateau, which can be attributed to the spherical diffusion at

nanoelectrodes. The curve at Pt-CS/GCE gave a bell-shape peak sited on a sloped baseline, which can be attributed to a surface enrichment effect of the nanoparticles at the electrode surface, which is obviously an advantage of the as-prepared electrode.

It is obvious from the comparison that the Pt-CS nano-composites can provide not only stronger catalytic ability than the single Pt nanoclusters but also have a surface enrichment effect to enhance the sensing ability. The enhancement of the catalytic ability can be from the reduction of the particle size and enlargement of the active surface area of the eletrodeposited Pt nanoparticles. These can be achieved from the coverage of the Pt nanoparticles with the chitosan films in nanometer thickness because of the inhibition of aggregation. Another factor may also be important is that the presence of chitosan coverage introduces many active functional groups such as amino and hydroxyl groups to the surface of the nanoparticles. In addition, the amino groups can be protonation in acidic solution, which can be attracted by the negatively charged NO_2^- anions in result of surface accumulation of nitrite ions to enhancing the sensing ability.

Scan rate dependence of the peak current. The effect of scan rate on the peak current of NO_2^- at Pt-Cs/GCE was investigated, as shown in Figure 6(a). It shows that the peak current (i_{pa}) was a linear function of the scan rate (v) in the range up to 50 mV/s, and bias from this relationship when the scan rate was higher. However, the i_{pa} was also a linear function of $v^{1/2}$ over the range of 10 – 100 mV/s, i_{pa} (μA) = 4.70 + 2.31 [v (mV/s)]$^{1/2}$ with a correlation coefficient (R) of 0.998. This result suggests a diffusion–controlled process with certain amount of surface accumulation.

For a totally irreversible diffusion-controlled system, the anodic peak potential can be represented by Eq. (1) [23]:

$$E_p = 2.3RT / (1 - \alpha)n_aF \log v + K \qquad (1)$$

where α is the transfer coefficient, n_a the number of electrons involved in the rate-determining step, K is a constant and the remaining symbols have their usual meanings.

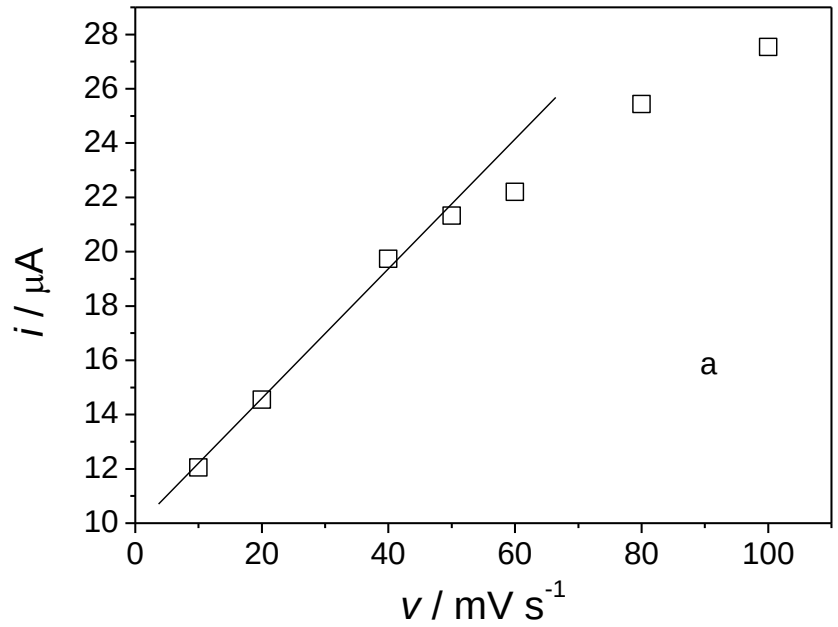

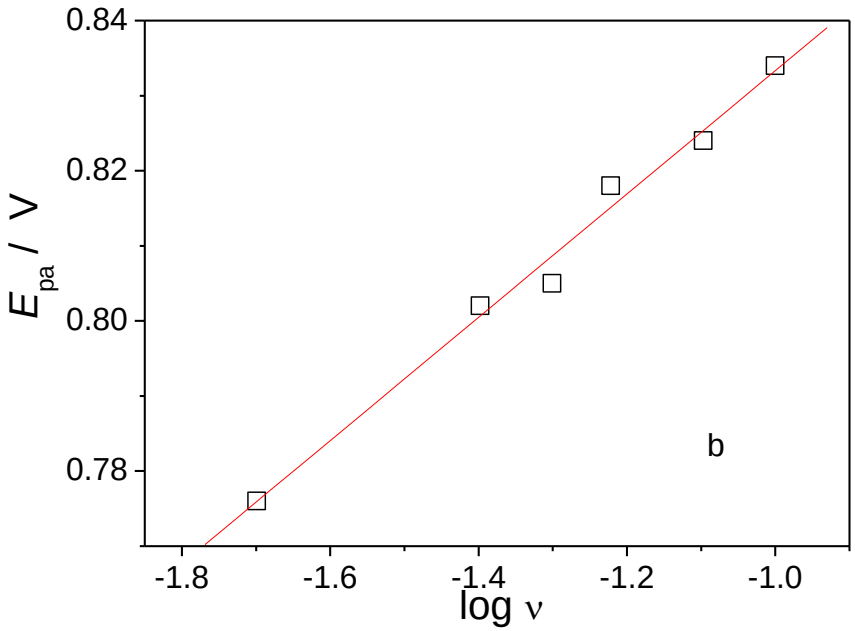

Figure 6. Plot of i_{pa} vervus the scan rate (a) and E_{pa} versus the square root of scan rate (b) at Pt-CS/GCE in 0.50 mM $NaNO_2$ + 0.1 M PBS (pH 6.0).

Based on the slope of E_p versus log(v), shown in Figure 6(b), the Tafel slope of 164 mV/decade was obtained and $(1-\alpha)n_\alpha$ was calculated to be 0.35, from which n_α=1 and α=0.65 were suggested. The Tafel slopes much greater than the normal 30–120 mV/decade have been related either to chemical reactions coupled to electrochemical steps or to substrate–catalyst interactions in a reaction intermediate [24]. The intermediate value of the Tafel slope obtained in this work suggests a weaker substrate–catalyst interaction at the nanocomposites. Ultimately, the total number of electrons (n) involved in the electrocatalytic oxidation of nitrite was evaluated according to Eq. (2) for totally irreversible diffusion-controlled processes [23]:

$$I_p = 2.99 \times 10^5 n[(1-\alpha)n_a]^{1/2} AC_0 D^{1/2} v^{1/2} \qquad (2)$$

where A is the area of the electrode, C_0 is the concentration of the electroactive reactant, D is the diffusion coefficient. Using $D=1.6\times10^{-5}$ cm^2 s^{-1} for nitrite ion [25], A=0.126 cm^2, n=2 was obtained, which is in agrrement with the mechanism of two electrons oxidation of nitrite (NO_2^-) to generate nitrate (NO_3^-).

The effect of pH. The pH effect on the NO_2^- oxidation at Pt-CS /GCE was investigated using DPV, as shown in Figure 7. The anodic peak potential was reduced (shifted to negative direction) with increasing from pH 3 to pH 6, and then increased back from pH 6 to pH 10 (Fig. 7A), revealing the optimal pH value for electrocatalytic oxidation of nitrite should be pH 6. Also, the current sensitivity also showed the optimal value at pH 6 (Fig. 7B). This is reasonable because the amino group in chitosan has a pKa value of ~6.5, thus, about one half of the chitosan can be positively charged due to

protonation at pH 6, which benefits to accumulate negatively charged NO_2^- anions, whose concentration is increased with pH increasing and becomes dominate form for pH>4. In addition, the conversion of NO_2^- to NO at low pH may occur [26]. Therefore, the optimum solution pH was selected as pH 6.0 for further study.

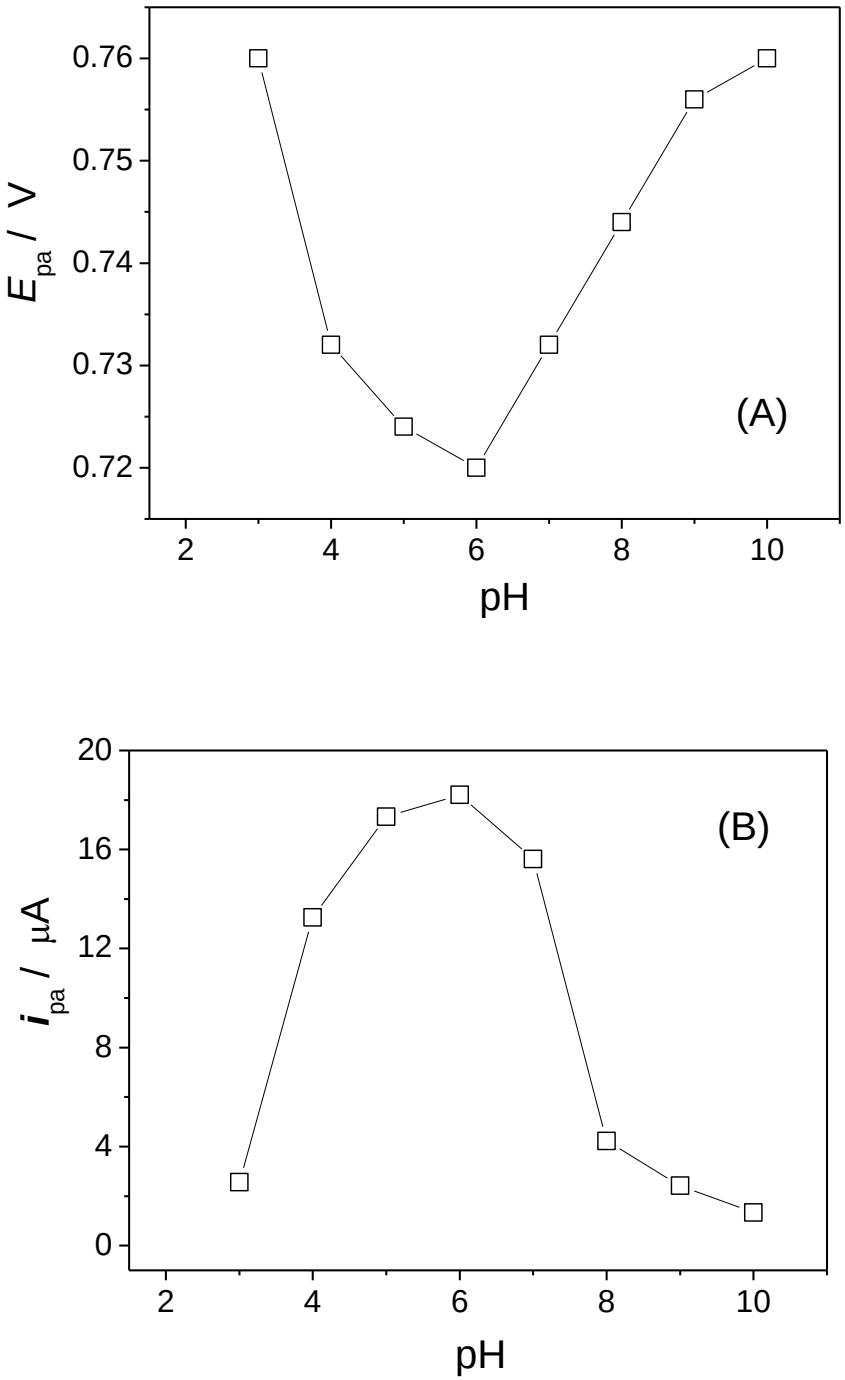

Figure 7. Effect of pH on E_{pa} (A) and i_{pa} (B) for the oxidation of 0.5 mM $NaNO_2$ at Pt-CS/GCE. DPV parameters: scan rate = 50 mV/s, amplitude = 50 mV, pulse width = 50 ms, pulse period = 200 ms.

The effect of the electrodeposition conditions. The effect of the concentration of H_2PtCl_4 and the concentration chitosan in the deposition solution on the sensing response of NO_2^- was investigated at fixed CV scan rate and cycles. We found that the response of the sensor increases with the increase of concentration for both substances, chitosan and H_2PtCl_4 at lower concentration range and then decreases with further increase of the concentration, and the maximal response was at concentration of 2.0 mM H_2PtCl_4 and 0.5% chitosan. Because an increase of the thickness of the CS coverage may increase the surface accumulation ability and protection ability, thus benefit the current sensitivity and sensor stability, however, it could reduce the conductivity between the Pt cores and the GCE substrate, thus reduce the sensing ability, the chitosan concentration should be well controlled by using the optimal value for the electrode fabrication.

Nitrite detection. The calibration curve for DPV determination of nitrite at Pt-CS/GCE is shown in Figure 8. The DPV peak current (I_p) was a linear function of nitrite concentration in the wide range of 9.9×10^{-7} to 7.5×10^{-3} M, I_p (μA) = 1.742+ 0.0215 $c_{nitrite}$(μM) (R = 0.999).

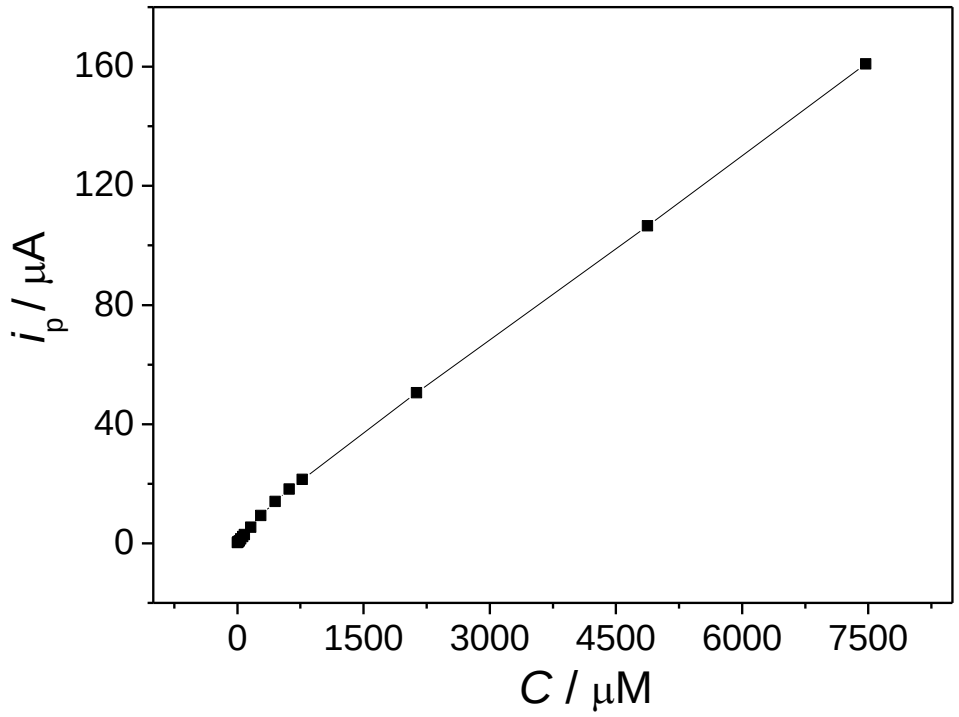

Figure 8. Plot of the linear calibration curve for DPV determination of $NaNO_2$.

A detection limit (s/n=3) of 1.50×10^{-7} M was determined. The advantage of the Pt-CS/GCE can be attributed to the structure of the electrodeposited Pt-CS nano-composite. As described above, the core-shell structure of the Pt-CS nano-composite has stabilized Pt nanoparticle core that enlarges the active surface area of the catalyst, and the nano-thickness chitosan shell coverage brings dense -NH_2^+ groups on the Pt surface, which can accumulate nitrite anions through molecular interactions, promoting the reaction reversibility and current sensitivity.

Interferences , Reproducibility and stability. The anti-interference ability of the Pt-CS/GCE was investigated. The criterion of the interference is based on the DPV current response. If the addition of given molecules or ions causes a current change of 10% or more, we consider it to interfere. In the experiments of testing for the possible interference, a 5×10^{-4} M nitrite was used. We found that 200-folds Na^+, K^+, Ca^{2+}, SO_4^{2-}, Mg^{2+}, NO_3^- and Cl^- did not interfere with the determination of nitrite. Although dopamine, uric acid and ascorbic acid were electroactive species, they did not interfere in the same concentration of nitrite since their oxidation potentials were far apart from the nitrite oxidation.

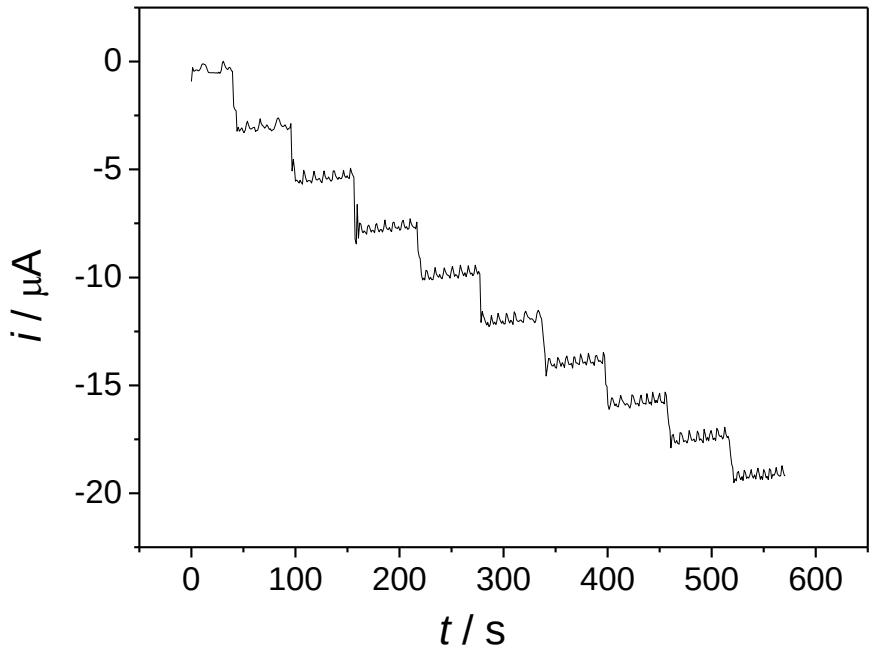

Figure 9. DPA response of Pt-CS/GCE with successive addition of 0.10 mM $NaNO_2$ in a stirred solution of 0.1 M PBS (pH 6.0)

The differential pulse amperometry (DPA) was also conducted for nitrite determination as shown in Figure 9. For successive additions of nitrite (0.1mM each time) by injection of 10 μl of 0.1M nitrite into 10 ml PBS, the response time of the as-prepared electrode was about 3 s for each addition and the current steps showed excellent reproducibility. The current response of the electrode exhibited almost no change for 2 week during the storage in the air. An 80% response current still retained after 30 days. The fabricated electrode showed good sensitivity, reproducibility, and stability.

4. CONCLUSIONS

In the present work, a platinum-chitosan nano-composite (Pt-CS) has been prepared by simple electrochemically co-deposition on GCE surface for fabrication of nitrite sensor, Pt-CS/GCE. The Pt-CS nanocomposite was stable and homogeneously distrubuted on the surface of substrate, showing

average size of 250 nm, which is constructed by several Pt-CS core-shell structures in about 8.5 nm in diameter. The presence of chitosan forming nanothickness coverage is a key factor for the formation of homogenously distributed and stable nano-sized Pt nanoparticles with high catalytic activity towards the oxidation of nitrite, which contains amino functional groups that can provide molecular interactions with nitrite anions to accumulate them on the surface of the nanopartical catalyst. The electrode easily prepared has a high electro-catalytic activity toward nitrite oxidation by further reducing the overpotential and has good sensing ability by significant enhancement of the CV and DPV peak current response of nitrite oxidation in comparison with simply Pt nanoclusters modified electrode. The obtained electrode exhibited good reproducibility and stability for the oxidation of nitrite. This one-step co-deposition of core-shell nanocomposite structure for fabrication of surface modified electrodes is simple and efficient and may find further applications in the field of electrochemical sensing.

ACKNOWLEDGEMENT
This work was supported financially by the Natural Science Foundation of Educational Department of Anhui Province (No. KJ2012Z328), the Foundation for Young Talents in College of Anhui Province under Grant No.2012SQRL166, the National Natural Science Foundation of China (Grant No.21103040) and Hefei Normal University

References

1. H. Wang, X. G. Bo, J. Bai, X. Wang, l. P. Guo, *J. Electroanal. Chem*., 662 (2011) 281.
2. M. H.Yang,Y. H. Yang,Y. L. Liu, G. L. Shen, R. Q. Yu, *Biosens. Bioelectron*., 21 (2006) 1125.
3. X. H. Kang, Zh.B Mai , X.Y.Zou, P.X. Cai, J.Y. Mo, *Talant*a,74 (2008) 879.
4. Y.X. Li, Y. Zhou, H.Y. Xian, L. Wang, J.Q. Huo, *Anal. Sci*., 27(2011) 1223.
5. Ch. X. Zhang, J. Hu, X. K. Wang, X.D. zhang, H. Toyoda, M. Nagatsu, Y.D. Meng, Carbon,50(2012)3731.
6. Y. P. He, Q. L. Sheng, J. B. Zheng, *Sensor Actuat B-Chem*, 166-167(2012)89.
7. H. M. zhang, F. X. Jiang, R. Zhou,Y.K. Du, P. Yang, C.Y. Wang, J.K. Xu, *Int. J. Hydrogen Energy*, 36(2011)15052.
8. Zh. Y. Wu, L.G. Chen, G. L. Shen, R.Q.Yu, *Sensor Actuat B-Chem*, 119(2006)295.
9. H. Z.Huang,Q.Yuan, X. R.Yang, *Colloid Surface* B ,39(2004)31.
10. D. S. Santos, P. J. G.Goulet, N. P. W.Pieczonka, *Langmuir* 20(2004)10273.
11. K.Esumi, N.Takei,T.Yoshimura, *Colloid Surface* B ,32(2003)117.
12. Ch. F. Ou, R.Yuan, Y.Q.Chai, M.Y. Tang, R.Chai, X.L. He, *Anal. Chim. Acta*., 603 (2007) 205.
13. H. Z. Huang, X. R. Yang , *Colloid Surface* A,226(2003)77.
14. M. Mathew, S. Sureshkumar, N. Sandhyarani , *Colloid Surface* B ,93(2012)143.
15. D. Feng, F. Wang, Z. L. Chen, *Sensor Actuat B-Chem*, 138(2009)539.
16. Zh. D. Wang, X. G. Hao, Zh. G. Zhang, Sh. B. Liu, Zh. H. Liang, G.Q. Guan, *Sensor Actuat B-Chem*, 162(2012)353.
17. A. C. Hill, R. E. Patterson, J. P. Sefton, and M. R. Columbia, *Langmuir* 15(1999) 4005.
18. Y. H. Xu, X.Q. Lin, *Electrochimi Acta, 52(2007)5140.*
19. C. L.Schauer, M. S. Chen, et al, *Thin Solid Films*, 434(2003) 250.
20. E. Khaled1, H.N.A. Hassan1, I.H.I. Habib and R. Metelka, *Int. J. Electrochem. Sci*., 5 (2010) 158.
21. J. E.Park, , S. G. Park, *Synthetic. Met*., 141(2004)265.

22. V. Radmilovic, H. A. Gasteiger, *J. Catal.* 154(1995)98.
23. A. J. Bard, and L. R. Faulkner, Electrochemical Methods, Fundamentals and Applications , Wiley, New York(1980).
24. P. Tau, T. Nyokong , *J. Electroanal. Chem*., 611 (2007) 10.
25. B. Piela, P.K. Wrona, *J. Electrochem. Soc*, 149(2002) E55.
26. B. Keita, A. Belhouari, L.Nadjo, R. Contant, *J. Electroanal. Chem.*, 381(1995)243.